https://doi.org/10.5194/egusphere-2025-6257
Preprint. Discussion started: 14 January 2026

Variability and trends of upper-tropospheric aerosols over the Asian summer monsoon region: An AeroCom multi-model study

Mian Chin[1], Jonathon S. Wright[2,3], Huisheng Bian[1,4], Qian Tan[5,6], Xiaohua Pan[1,7], Toshihiko Takemura[8], Hitoshi Matsui[9], Kostas Tsigaridis[10,11], Susanne Bauer[11], Paul Ginoux[12], Yiran Peng[2,3], Zengyuan Guo[13,3], Suvarna Fadnavis[14], Anton Laakso[15], John P. Burrows[16], Ghassan Taha[1,17], Jayanta Kar[18,19], Alexei Rozanov[16], Carlo Arosio[16], Landon Rieger[20], Adam Bourassa[21]

[1]NASA Goddard Space Flight Center, Greenbelt, Maryland, USA
[2]Department of Earth System Science, Tsinghua University, Beijing, China
[3]Ministry of Education Key Laboratory for Earth System Modeling, Tsinghua University, Beijing, China
[4]University of Maryland Baltimore County, Baltimore, Maryland, USA
[5]Bay Area Environmental Research Institute, Moffett Field, California, USA
[6]NASA Ames Research Center, Moffett Field, California, USA
[7]ADNET Systems, Inc., Bethesda, Maryland, USA
[8]Research Institute for Applied Mechanics, Kyushu University, Kyushu, Japan
[9]Graduate School of Environmental Studies, Nagoya University, Nagoya, Japan
[10]Center for Climate Systems Research, Columbia University, Palisades, New York, USA
[11]NASA Goddard Institute for Space Studies, New York, New York, USA
[12]NOAA Geophysical Fluid Dynamics Laboratory, Princeton, New Jersey, USA
[13]Climate Studies Key Laboratory, National Climate Center, China Meteorological Administration, Beijing, China
[14]Indian Institute of Tropical Meteorology, Pune, India
[15]Finnish Meteorological Institute, Kuopio, Finland
[16]Institute of Environmental Physics, University of Bremen, Bremen, Germany
[17]Morgan State University, Baltimore, Maryland, USA
[18]Analytical Mechanics Associates, Hampton, Virginia, USA
[19]NASA Langley Research Center, Hampton, Virginia, USA
[20]Environment and Climate Change Canada, Victoria, British Columbia, Canada
[21]University of Saskatchewan, Saskatchewan, Canada

Correspondence to: Mian Chin (mian.chin@outlook.com)

Abstract. Aerosols in the upper troposphere play an important role in Earth's radiative balance and atmospheric composition. Satellite observations have revealed a recurrent enhancement of aerosol extinction coefficient (AEC) in the upper troposphere and near the tropopause over the Asian summer monsoon (ASM) anticyclone (ASMA) region during July–August. However, substantial uncertainties remain regarding (i) the influence of ASM dynamics and climate variability on these aerosols, (ii) the extent to which the upper-tropospheric aerosol trends reflect changes in surface pollutant emissions, and (iii) the ability of global models to simulate aerosol amounts, variability, and key controlling processes in the upper-tropospheric ASMA region. Here, we present results from an AeroCom-coordinated global multi-model study addressing these issues. Using simulations from nine models for 2000–2018, we find large inter-model differences in non-volcanic AEC over the upper-tropospheric ASMA region, with coefficients of variation ranging from 64% to 86%. Approximately half of this spread is attributable to differences in transport and wet removal processes, as diagnosed using common tracers, with discrepancies in wet removal contributing about eight times more than those associated with transport. The multi-model ensemble indicates an overall increase in non-volcanic AEC over the past two decades, consistent with rising anthropogenic emissions in Asia, while interannual variability is linked to climate variability as represented by the Multivariate ENSO Index. Through comparison with satellite observations, we further identify persistent model deficiencies, particularly in the representation of volcanic aerosols, and highlight priorities for future coordinated model developments and evaluation.

https://doi.org/10.5194/egusphere-2025-6257
Preprint. Discussion started: 14 January 2026

1 Introduction

The upper troposphere is a crucial region of the Earth's atmosphere, serving as an efficient pathway for material originating in the lower troposphere to spread across hemispheric scales and, at times, into the lower stratosphere. Aerosols in this region affect radiative forcing, cloud microphysics, and chemical composition, yet their sources, transport pathways, and variability remain less understood than those of gas-phase species.

The Asian Summer Monsoon (ASM) exerts strong control on upper-tropospheric composition. Deep convective heating during June-August drives a prominent upper-level anticyclonic circulation (ASM anticyclone, ASMA), bounded by the subtropical westerly jet to the north and the tropical easterly jet to the south (e.g., Gettleman et al., 2004; Randel et al., 2010; Vogel et al., 2014; Legras and Bucci, 2020). Convective lofting transports pollutants from the highly polluted Asian boundary layer into the upper troposphere, where they are spread out within the ASMA (Randel and Park, 2006, Park et al., 2007; Santee et al., 2017). Meanwhile, the dynamical instability of the ASMA further results in frequent eddy shedding toward both the east and west, carrying pollutants beyond the ASMA boundary (e.g., Popovic and Plumb, 2001; Ungermann et al., 2016; Pan et al., 2016; Fadnavis et al., 2018; Wang et al., 2022). On a broader scale, the energetic ASM system also couples with the Walker and Hadley circulations and with the stratospheric Brewer-Dobson circulation (Ploeger et al., 2017; Yan et al., 2019), extending its influence far beyond the monsoon region.

Satellite observations of carbon monoxide (CO) and other trace gases provide clear evidence of monsoon-driven pollutant transport into the upper troposphere and near the tropopause (Kar et al., 2004; Li et al., 2005; Jiang et al., 2007; Park et al., 2007, 2009; Randel et al., 2010; Pan et al., 2016; Santee et al., 2017; Liang et al., 2025; Wright et al., 2025). Although the ASM convective transport of aerosols into the upper troposphere is generally considered to be less effective due to efficient wet scavenging of aerosols in monsoon precipitation, data from the space-borne Cloud-Aerosol Lidar with Orthogonal Polarization (CALIOP) instrument onboard the Cloud-Aerosol Lidar and Infrared Pathfinder Satellite Observations (CALIPSO) satellite have revealed a recurrent enhancement of aerosol extinction near the Asian tropopause during July-August, referred to as the "Asian Tropopause Aerosol Layer" (ATAL) (Vernier et al., 2011, 2015). ATAL has since become a major focus of observational and modeling studies, including recent aircraft and balloon field campaigns (e.g., Vernier et al., 2018; Yu et al., 2017; Fadnavis et al., 2017, 2019; Ma et al., 2019; Hanumanthu et al., 2020; Mahnke et al., 2021; Pan et al., 2025). Figure 1 shows the CO concentrations at 100 hPa from the Microwave Limb Sounder (MLS) instrument onboard the EOS-Aura satellite and the aerosol extinction coefficient (AEC) at 17 km (above sea level) from CALIOP for August 2010, both clearly showing a pronounced "hot spot" in the ASMA region (indicated by the white rectangular box in Fig. 1). Recent studies, using information from the NASA Modern-Era Reanalysis for Research and Applications version 2 (MERRA-2) system, have found that large-scale uplift of aerosols and CO during the peak monsoon season occurs in chimney-shaped stems over the densely populated mega-complex in northern India and southwestern China, which collectively vent the surface-generated pollutants upward to reach the upper troposphere and lower stratosphere (UTLS) (Lau et al., 2018; Gao et al., 2023). These studies have demonstrated the key role of ASM in shaping upper-tropospheric composition.

Asia has the highest anthropogenic emission rates of aerosols and precursor gases globally (e.g., Hoesly et al., 2018; Soulie et al., 2024), yet it remains uncertain as to what extent the upper tropospheric aerosol trend reflects the surface emission trends. Additionally, interannual variations in UTLS aerosol abundance arise from a complex interplay among transport, wet scavenging, chemistry, and circulation variability, which could differ substantially across the models and is challenging to evaluate observationally. Furthermore, it is also unclear how climate variability may regulate the upper tropospheric aerosol amount and variability.

https://doi.org/10.5194/egusphere-2025-6257
Preprint. Discussion started: 14 January 2026

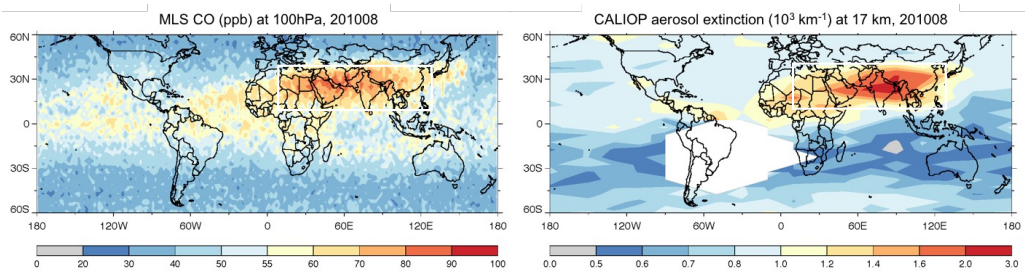

Figure 1: Satellite data of monthly composite of CO concentrations from Aura/MLS at 100 hPa (left; Aura MLS CO L2 V5) and AEC from CALIOP at 17 km (right; CALIOP L3 Stratospheric-APRO V1.00) for August 2010. The white rectangular box indicates the nominal ASMA region (10°N–40°N, 10°E–130°E, modified from Santee et al., 2017).

To address these issues, an internationally coordinated modeling effort was initiated in the framework of the Aerosol Comparisons between Observations and Models (AeroCom), namely the UTLS model experiment, which is a part of the AeroCom Phase-III studies. AeroCom is an open international initiative involving more than 20 global modeling groups and numerous observational teams, aimed at evaluating aerosol processes across models, identifying sources of model-observation differences, and accessing a wide range of aerosol environmental impacts (https://aerocom.met.no/).

This study reports results from the AeroCom UTLS model experiment to study the aerosol variability and trends in the upper troposphere with multiple global model simulations (https://aerocom.met.no/experiments/UTLS), a subject that had not been investigated in previous AeroCom studies. The AeroCom UTLS experiment was also developed in cooperation with the IGAC/APARC Atmospheric Composition and the Asian Monsoon (ACAM) activity. In that context, our present study focuses on the upper tropospheric ASM region to (1) evaluate the multi-model simulated AEC against available satellite observations; (2) diagnose inter-model differences in AEC and quantitatively attribute them to differences in transport and removal processes; and (3) quantify two-decadal (2000–2018) trends and interannual variability of aerosols and assess their relationships with anthropogenic emissions, transport, removal, and climate variability.

The model experiment setup and satellite AEC datasets are described in Sect. 2. Results are presented in Sect. 3, including model-observation comparisons, process attribution using diagnostic tracers, and assessments of aerosol trends and variability. Outstanding issues and broader implications are discussed in Sect. 4, followed by conclusions in Sect. 5.

2 AeroCom UTLS model experiment and data source

2.1 Description of the UTLS model experiment

The AeroCom UTLS model experiment comprises global simulations from 2000 to 2018 (19 years). All models were required to use the same prescribed emissions from anthropogenic, biomass burning, and volcanic sources, whereas emissions of desert dust, sea salt, and biogenic sources were calculated or specified by each model individually. Emissions from anthropogenic and biomass burning sources were taken from those prepared for the Coupled Model Intercomparison Project phase 6 (CMIP6), i.e., the anthropogenic emissions from the Community Emission Data System (CEDS) for 2000–2014 (Hoesly et al., 2018) and biomass burning emission from the Global Fire Emission Dataset version 4s (GFED4s) for 2000–2015 (van Marle et al., 2017). For the later years in our study period, CMIP6 emissions were unavailable; therefore, the 2014 anthropogenic emission from CMIP6 was also used for 2015–2018 model simulations as a practical approach. Additionally, the GFED4.1s (van der Werf et al., 2017) biomass burning emission was used for 2016–2018 model simulations to maintain continuity. Species emitted from anthropogenic and biomass burning sources included primary aerosols of black carbon (BC) and organic carbon (OC) as well as precursor gases for secondary aerosols, including sulfur dioxide (SO_2), nitrogen oxides (NO_x), ammonia (NH_3), and volatile organic compounds

https://doi.org/10.5194/egusphere-2025-6257
Preprint. Discussion started: 14 January 2026

(VOC). Volcanic emissions of SO_2 amount and plume top height were from satellite-based estimation (Carn et al., 2015, 2017) with 2000-2003 based on EP-TOMS observations and 2004-2018 based on Aura-OMI, including both sporadically erupting and degassing volcanic emissions. Emissions from other natural sources, such as biogenic, dust, and sea salt were calculated by individual models.

The modeling approach involved a baseline simulation (BASE) with emissions from all sources and two tiers of sensitivity simulations: Tier-1 targeted aerosol source types globally by excluding anthropogenic (ANT0), biomass burning (FIR0), and volcanic (VOL0) emissions, whereas Tier-2 specifically targeted anthropogenic emissions in East Asia (EAS0) and South Asia (SAS0).

All modeling groups were further requested to implement a suite of tracers for diagnosing inter-model and interannual differences in transport and aerosol removal. The prescribed sources for the tracers were used repeatedly for all simulated years (2000-2018). The transport tracer is a CO-like species, TR_{CO50}, with prescribed CO sources including direct emissions of CO from anthropogenic and biomass burning activities with the 2010 CMIP6 emission, as well as prescribed secondary sources from chemical productions of non-methane VOC (NMVOC) and from methane oxidation. The sink of TR_{CO50} is also prescribed at a 50-day atmospheric lifetime. Because the source and sink of TR_{CO50} are identical in all years and in all models, the inter-model and interannual differences in the simulated spatiotemporal distributions of TR_{CO50} should be exclusively attributed to the differences in transport processes associated with the meteorological conditions.

The aerosol removal is tracked by a pair of lead (^{210}Pb) and radon (^{222}Rn) tracers, referred here as TR_{Pb} and TR_{Rn}, respectively. TR_{Pb} is produced in the atmosphere from TR_{Rn} decay and is removed after attachment to fine-mode aerosols, which are predominantly lost to wet scavenging by rain and clouds in the atmosphere (Balkanski et al., 1993; Liu et al., 2001). The prescribed TR_{Rn} is emitted from global land areas (Zhang B. et al., 2021, modified from Zhang K. et al., 2011) and experiences radioactive decay at a prescribed lifetime of 5.5 days to form TR_{Pb}. TR_{Pb} is then removed by dry and wet depositions following the treatment for sulfate aerosol in each model. We use the TR_{Pb} to TR_{Rn} ratio, denoted as $TR_{Pb/Rn}$, to diagnose the efficiency of removal processes – a lower value of $TR_{Pb/Rn}$ indicates more efficient removal of aerosol.

Table 1 summarises the AeroCom-III UTLS Tier-1 requirements and implementations. More details for the requirements of UTLS experiment and diagnostic tracers can be found at https://aerocom.met.no/experiments/UTLS/ and https://aerocom.met.no/data/data-submission/, respectively. In this study, we analyze the result from BASE and VOL0 experiments to focus on the aerosols originating from tropospheric sources.

Global model simulations performed by nine modeling groups from the US, Japan, China, and India/Finland were submitted for the AeroCom UTLS model experiment (Table 2), although some models have only performed subsets of the Tier-1 model experiment listed in Table 1. Among the models, only GEOS-i33p2 included "background" sulfate aerosol produced from carbonyl sulfide (OCS) oxidation, which is an important source of aerosols in the stratosphere.

Table 1. AeroCom UTLS model experiment Tier 1 requirements.

Simulation years:		2000–2018, monthly output for aerosols and related species
Experiments	BASE:	All emissions (anthropogenic, biomass burning, volcanic, biogenic, dust, sea salt)
	VOL0:	Same as BASE except no volcanic emissions
	FIR0:	Same as BASE except no biomass burning emissions
	ANT0:	Same as BASE except no anthropogenic emissions
Transport tracer TR_{CO50}:		Sources: prescribed 12-monthly CO emissions. Sink: Prescribed 50-day lifetime
Removal tracer, ratio of TR_{Pb} to TR_{Rn} ($TR_{Pb/Rn}$):		TR_{Rn}: Prescribed ^{222}Rn emission, radiative decay (5.5-day lifetime) to form ^{210}Pb TR_{Pb}: Formed from ^{222}Rn decay, removed by dry/wet deposition treated as sulfate

https://doi.org/10.5194/egusphere-2025-6257
Preprint. Discussion started: 14 January 2026

Table 2. Participating models in AeroCom UTLS model experiment.

Model (Institute)	lon°× lat°× #lev	Meteorology	Tier 1 Exp. submitted	Tracers	References
GEOS-i33p2 (NASA GSFC, USA)	1°× 1°× 72	Replay MERRA-2	BASE, VOL0, ANT0, FIR0	Yes	Chin et al. (2009); Colarco et al. (2010)
CIESM-MAM7 (Tsinghua Univ., China)	2.5°×1.875°×30	Forced by SST	BASE, VOL0, ANT0, FIR0,	Yes	Lin et al. (2020)
GISS-OMA[1] (NASA GISS, USA)	2.5°×2°×40	Nudged by MERRA-2	BASE, VOL0, ANT0, FIR0,	Yes	Koch et al. (2006); Tsigaridis et al. (2013)
GISS-MATRIX[1] (NASA GISS, USA)	2.5°×2°×40	Nudged by MERRA-2	BASE, VOL0, ANT0, FIR0,	Yes	Bauer et al. (2008)
GFDL-fSST[1] (NOAA GFDL, USA)	1.25°×1°×33	Forced by SST	VOL0[2]	Yes	Zhao et al. (2018)
GFDL-nSST[1] (NOAA GFDL, USA)	1.25°×1°×33	Forced by SST & nudged by NCEP winds	VOL0[2]	Yes	Zhao et al. (2018)
CAM5-ATRAS (Nagoya Univ., Japan)	2.5°×1.875°×30	Nudged by MERRA-2	BASE, VOL0, ANT0, FIR0,	Yes	Matsui (2017); Matsui and Mahowald (2017)
MIROC-SPRINTARS (Kyushu Univ., Japan)	0.56°×0.56°×40	Nudged by ERA5 winds, temperature, pressure	BASE, VOL0, ANT0, FIR0	Yes	Takemura et al. (2005)
ECHAM6-HAMMOZ (IIT, India | FMI, Finland)	1.875°×1.875°×47	Forced by SST	BASE, VOL0, ANT0, FIR0	No	Schultz et al. (2018); Fadnavis et al. (2019)

[1]Complete model names: GISS-ModelE2p1p1-OMA, GISS-ModelE2p1p1-MATRIX, GFDL-AM4-fSST, GFDL-AM4-nSST.
[2]Because the GFDL BASE contributions do not include volcanic emissions, BASE simulations for this model are designated VOL0.

2.2 Satellite aerosol extinction data in the UTLS

Satellite retrievals of aerosol vertical profiles in the UTLS are available from both active sensors (e.g., lidar) and the limb-scatter instruments. In this study for evaluating BASE model simulations, we use the Level-3 (L3) monthly gridded AEC products from the space-borne lidar CALIOP on the CALIPSO satellite (Kar et al., 2019) and from three limb-scatter instruments: the Optical Spectrograph and InfraRed Imaging System (OSIRIS) on the Odin satellite (Bourassa et al., 2012; Rieger et al., 2015, 2019), the Scanning Imaging Absorption Spectrometer for Atmospheric Chartography (SCIAMACHY) on the Envisat satellite (Burrows et al., 1995; Bovensmann, 1999; Malinina et al., 2018; Noël et al., 2020), and the Ozone Mapper and Profiler Suite Limb Profiler (OMPS LP) on the Suomi-NPP satellite (Taha et al., 2021). Table 3 lists brief information about these products.

Table 3. Satellite products of aerosol extinction coefficient profiles in the UTLS.

	OSIRIS	SCIAMACHY	OMPS LP	CALIOP
Timeframe	2001–present	2002–2012	2012–present	2006–2023
Aerosol extinction product	Limb-scatter measurements of aerosol extinction profiles at 750 nm, converted to 550 nm	Limb-scatter measurements of aerosol extinction profiles at 750 nm, converted to 550 nm	Limb-scatter measurements of aerosol extinction profiles at multi-wavelength	Laser measurements of aerosol backscatter converted to extinction at 532 nm
Spatial coverage	Cloud top to 35 km	Cloud top to 38 km	Cloud top to 40 km	Tropopause to 36 km
Data version	Version 7.0 daily gridded profiles	Version 3.0 daily gridded profiles	Version 2.1 (NASA) daily gridded profiles	Strat_V1-00 monthly gridded profiles
L3 spatial resolution	30° lon, 5° lat, ~2 km vertical	15° lon, 5° lat, 3-4 km vertical	20° lon, 1.5° lat, 1 km vertical	20° lon, 5° lat, 0.9 km vertical

Among the satellite products, OSIRIS provides the longest data overlap (2001-2018) with our study period of 2000-2018, followed by CALIOP (mid 2006-2018), SCIAMACHY (2002–2012), and OMPS LP (2012–2018). AEC products from the limb-scatter instruments at 750 nm are converted to 550 nm by multiplying a factor of 2.2 (based on typical Ångström Exponent) while AEC

https://doi.org/10.5194/egusphere-2025-6257
Preprint. Discussion started: 14 January 2026

from CALIOP is used at its native wavelength of 532 nm. Retrievals of AEC in the upper troposphere and near the tropopause are especially challenging due to the frequent co-existence of aerosols and cirrus clouds, which limits the reliability and representativeness of aerosols retrieved from the measured signals (e.g., Kremser et al., 2016; Langille et al., 2025).

3 Results

3.1 Comparisons of AEC between observations and models in the UTLS ASMA region

We compare the time-series of monthly mean AEC at 550 nm (2002–2018) from the model BASE simulations with four satellite products in the ASMA region (10°N–40°N latitude and 10°E–130°E longitude, see closed rectangular area in Fig. 1) at altitudes near the tropopause (~100 hPa or 16.5 km, Fig. 2) and in the lower stratosphere (~70 hPa or 19.5 km, Fig. 3). At altitudes below the tropopause, satellite retrievals are subject to larger uncertainties with little L3 data available over the ASMA region because of increased cloud presence, which makes aerosol retrievals more difficult.

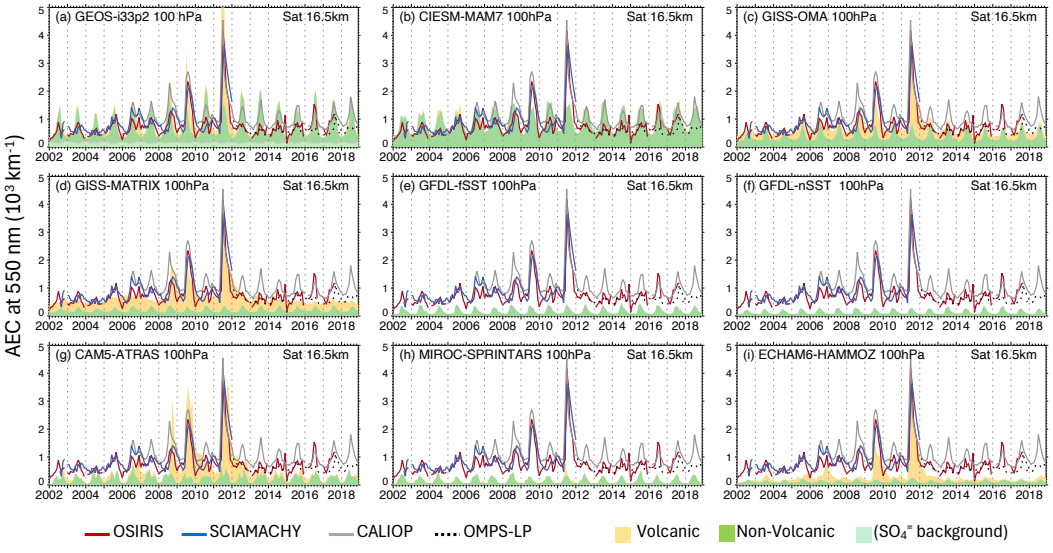

Figure 2: Comparisons of monthly AEC (2002–2018) near the tropopause over the ASMA region from nine participating models' BASE simulations at 100 hPa (color-shading) against those from four satellite products at 16.5 km altitude (lines). Model simulated non-volcanic and non-volcanic AEC are shown in green and yellow shadings, respectively. The light green shading in GEOS-i33p2 model (panel a) illustrates the contribution of "background" sulfate aerosol formed by OCS oxidation (not included by other models). Note that the GFDL models (panels e and f) does not include volcanic emissions in their BASE simulations.

The Tier-1 experiments support separation of aerosols simulated by each model into volcanic (yellow shading in Fig. 2 and 3) and non-volcanic (green shading) aerosols, where non-volcanic aerosols including anthropogenic, biomass burning, and other natural aerosols. Several features emerge from Fig. 2 and 3: First, model-simulated non-volcanic aerosols display clear seasonal cycles near the tropopause (Fig. 2) and in the lower stratosphere (Fig. 3), with maximum values in boreal summer and minimum values in boreal winter. This seasonal cycle results mostly from the Asian summer monsoon convective transport, although the amount of non-volcanic aerosol reaching the tropopause and lower stratosphere differs considerably among the models with highest amount in CIESM-MAM7 (panel b) and lowest amount in GFDL (panels e and f). Second, aerosols from eruptive volcanoes (e.g., Sarychev Peak in the Kuril Islands of Russia in 2009, Nabro in the Southern Red Sea Region of Eritrea in 2011) cause significant perturbations in aerosol amount and large year-to-year variations at these altitudes. However, even though all models use the same emissions (described in Sect. 2.1), differences in implementations of volcanic aerosol simulations (such as injection heights and

https://doi.org/10.5194/egusphere-2025-6257
Preprint. Discussion started: 14 January 2026

sulfate formation rates from volcanic SO_2 oxidation) produce large differences in volcanic AEC near the tropopause and in the lower stratosphere. For example, whereas volcanic influences are negligible in CIESM-MAM7 (panel b) and MIROC-SPRINTARS (panel h) even during years with large volcanic eruptions, GISS-MATRIX (panel d) model attributes more than 50% of AEC to volcanic aerosols at 100 and 70 hPa even during the years without large volcanic eruptions. Third, the GEOS-i33p2 (panel a) simulations suggest that the background sulfate aerosol from OCS oxidation is a major contributor to the stratospheric aerosol, accounting for 70-80% of non-volcanic AEC at 70 hPa (Fig. 3), although this source has a minor contribution (about 10%) at 100 hPa (Fig. 2). Lastly, there are also clear differences among the satellite AEC products, with AEC from CALIOP (grey line) generally higher than that from other satellite retrievals near the tropopause (Fig. 2), although the inter-satellite differences are much smaller than the inter-model differences.

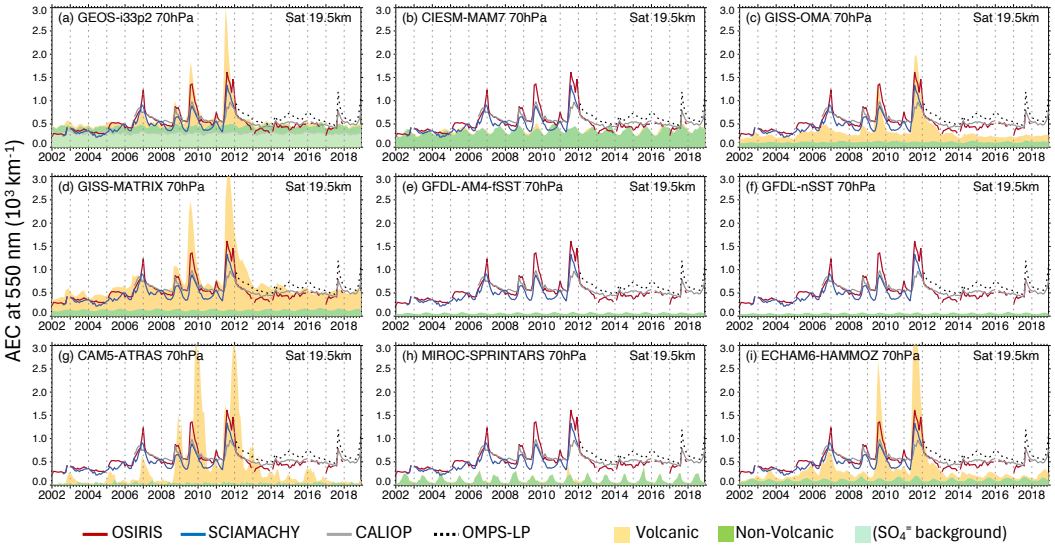

Figure 3: Same as Fig. 2 but at 70 hPa for models and 19.5 km for satellite products.

To mitigate the differences resulting from the model implementations of volcanic and background aerosols that do not play significant roles in linking aerosols in the upper troposphere with ASM dynamics, the remainder of this study focuses on model simulations of non-volcanic aerosols from VOL0 experiment at 150 hPa (a nominal altitude representing the upper troposphere). The objectives are to diagnose the inter-model differences associated with ASM processes and to assess the trends and variability of non-volcanic aerosols in the upper troposphere over Asia.

3.2 Model simulated non-volcanic aerosols in the upper troposphere

In this and next sections, we use the model simulations for August 2012 as a demonstrative case for analyzing the inter-model difference in the representation of summertime non-volcanic AEC in the upper troposphere (this section) and diagnosing the major causes of this difference (Sect. 3.3). Results for other years are summarized at the end of Sect. 3.3.

Monthly mean non-volcanic AEC at 550 nm in August 2012, based on the models' VOL0 simulations, are shown in Fig. 4 for horizontal distributions at 150 hPa and in Fig. 5 for longitude-pressure vertical extent in the 10°N–40°N latitudinal band. Most models capture the "hot spot" of the non-volcanic AEC over the ASMA region (enclosed rectangular box in Fig. 4) at 150 hPa, along with sharp vertical gradient between the surface and the UTLS with the highest AEC values below 500 hPa (Fig. 5). Nonetheless, we find substantial inter-model differences in the simulated magnitude of AEC at 150 hPa and the vertical gradient from surface to the UTLS. For example, GEOS-i33p2 (panel a) simulates a much stronger vertical intrusion of aerosol into the

https://doi.org/10.5194/egusphere-2025-6257
Preprint. Discussion started: 14 January 2026

UTLS over the ASM convective region than other models. In contrast, ECHAM6-HAMMOZ (panel i) displays the sharpest reduction of AEC from the surface to higher altitudes with lowest values in the free troposphere. As a result, mean AEC in the 150 hPa ASMA region differs by a factor of more than 20 between the highest (GEOS-i33p2, at 2.84 10^3 km^{-1}) and the lowest (ECHM6-
210 HAMMOZ, at 0.13 10^3 km^{-1}) model-simulated values.

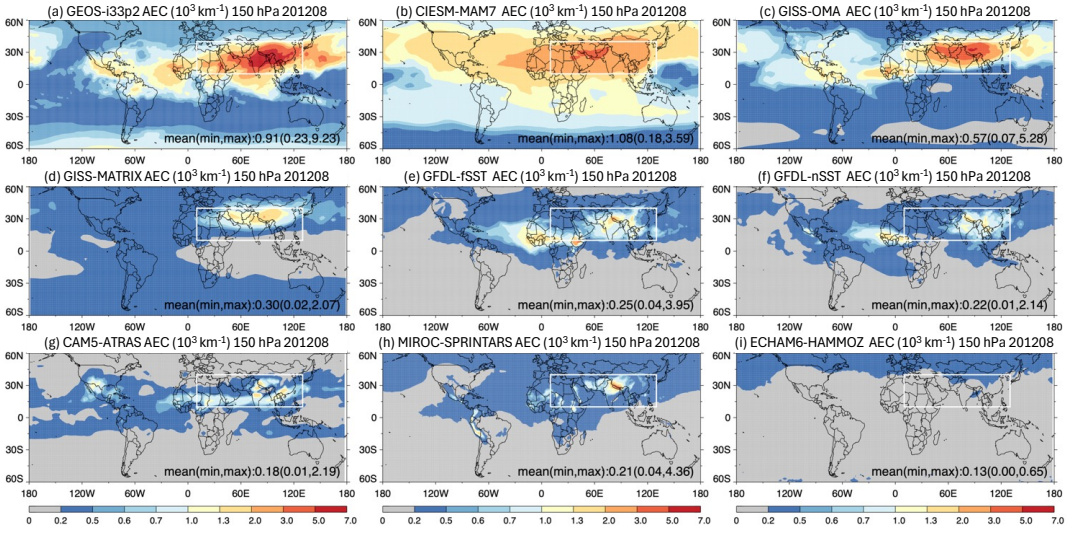

Figure 4: Model simulated non-volcanic AEC at 150 hPa in August 2012. The rectangular box represents the nominal boundaries of the ASMA region.

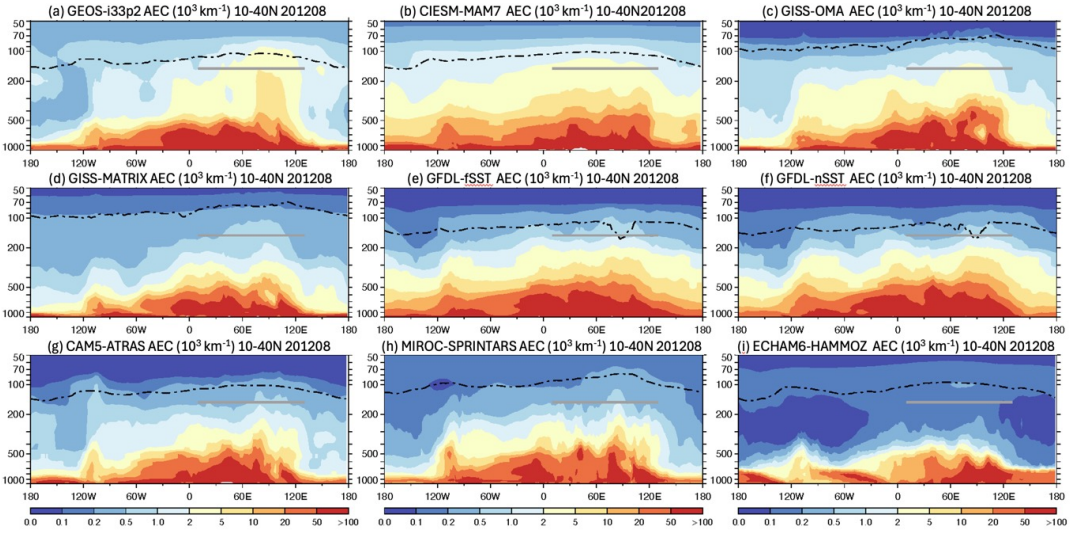

Figure 5: The longitude-pressure cross-section of model simulated non-volcanic AEC averaged within the 10°N-40°N latitude band in August 2012. The dash-dotted line shows the tropopause height from each model, and the grey solid line indicates the location of the ASMA region at 150 hPa.

Model-simulated magnitudes of non-volcanic AEC averaged over the ASMA region at 150 hPa for August 2012 are summarized in Table 4. The models can be separated into three groups based on their simulated mean ASMA AEC values: group A includes
215 (a) GEOS-i33p2, (b) CIESM-MAM7, and (c) GISS-OMA with simulated AEC values above 1.5 10^3 km^{-1}; group B includes (d)

https://doi.org/10.5194/egusphere-2025-6257
Preprint. Discussion started: 14 January 2026

GISS-MATRIX, (e) GFDL-fSST, (f) GFDL-nSST, (g) CAM5-ATRAS, and (h) MIROC-SPRINTARS with simulated AEC values around 0.5–0.7 10^3 km^{-1}); and group C includes (i) ECHAM6-HAMMOZ with a much lower AEC value at 0.13 10^3 km^{-1}. ECHAM6-HAMMOZ also exhibits a unique horizontal distribution at 150 hPa with no evident maximum above the ASM (see Fig. 3). We further calculate the coefficient of variation (CV) of AEC in the ASMA region among the models, defined as the ratio between the inter-model standard deviation (stdev) and multi-model mean (expressed as percentage), to provide a measure of the degree of inter-model spread. Previous studies have also referred to this metric as model "diversity" (Textor et al., 2006). We exclude the ECHAM6-HAMMOZ model from this calculation mainly because it does not provide the transport and removal tracer simulations necessary for diagnosing differences in model processes relevant to AEC (see Sect. 3.3 and 3.4). The multi-model mean AEC in the ASMA region from the eight models is 1.22 10^3 km^{-1} with a standard deviation of 0.96 10^3 km^{-1}, leading to a large CV value of 79%. (Table 4 also includes results for the transport and removal tracers, which will be discussed in Sect. 3.3.)

Table 4. Model-simulated non-volcanic AEC, TR_{CO50}, and $TR_{Pb/Rn}$ in August 2012 averaged over the ASMA region at 150 hPa.

	Model	AEC (10^3 km^{-1})	TR_{CO50} (ppb)	$TR_{Pb/Rn}$ (kg kg^{-1})
(a)	GEOS-i33p2	2.84	105.4	0.87
(b)	CIESM-MAM7	2.41	110.1	1.21
(c)	GISS-OMA	1.71	104.2	1.01
(d)	GISS-MATRIX	0.61	103.7	1.04
(e)	GFDL-fSST	0.69	106.9	0.44
(f)	GFDL-nSST	0.53	105.7	0.48
(g)	CAM5-ATRAS	0.50	98.2	0.79
(h)	MIROC-SPRINTARS	0.47	107.4	0.53
(i)	ECHAM6-HAMMOZ	0.13	-	-
	Mean (a–h)	1.22	105.2 (80.2)[1]	0.79
	Stdev (a–h)	0.96	3.5 (3.5)[1]	0.29
	CV (%) (a–h)	79%	3.3% (4.3%)[1]	36%

[1]Numbers in parenthesis are calculated with 25 ppb background TR_{CO50} value excluded.

Several major factors contribute to the large differences in model simulated AEC in the ASMA region despite all models using the same prescribed surface emissions. These factors include the processes related to convective transport of aerosols and precursor gases from the planetary boundary layer to the upper troposphere, removal of aerosols by wet scavenging, chemical production of secondary aerosols from their precursor gases during transport, and aerosol mass extinction efficiency (a function of aerosol chemical composition, particle size distribution, particle density, and hygroscopic growth, any of which may differ among models). In the following section, we diagnose inter-model differences in two of the most important processes contributing to model diversity, namely the convective transport (diagnosed using the pollutant transport tracer TR_{CO50}) and the wet removal (diagnosed with the aerosol removal tracer $TR_{Pb/Rn}$ computed as the ratio of TR_{Pb} to TR_{Rn}, as introduced in Sect. 2).

3.3 Inter-model differences in transport and removal process of aerosols

3.3.1 Diagnosing inter-model differences in transport process

Horizontal distributions of model-simulated transport tracer TR_{CO50} at 150 hPa for August 2012 are shown in Fig. 6. In contrast to the large inter-model differences in non-volcanic aerosol distributions presented in Fig. 4, TR_{CO50} concentrations from the models are much more similar. This similarity reflects identically prescribed emission and loss rates, the relatively long lifetime (50 days), and significant global "background" TR_{CO50} from prescribed methane oxidation (about 25 ppb globally) implemented in all models. (The relatively high TR_{CO50} concentrations over southern hemispheric Africa in MIROC-SPRINTARS (panel h) is caused by an

https://doi.org/10.5194/egusphere-2025-6257
Preprint. Discussion started: 14 January 2026

245 implementation issue related to the biomass burning source.) The lower right panel in Fig. 6 is the monthly composite of CO concentrations at 147 hPa from the Aura/MLS instrument for reference, although quantitative differences are subject to the caveat that TR_{CO50} is a tracer with prescribed sources and sinks while MLS CO represents the CO in the real-world resultant from the complex atmospheric processes.

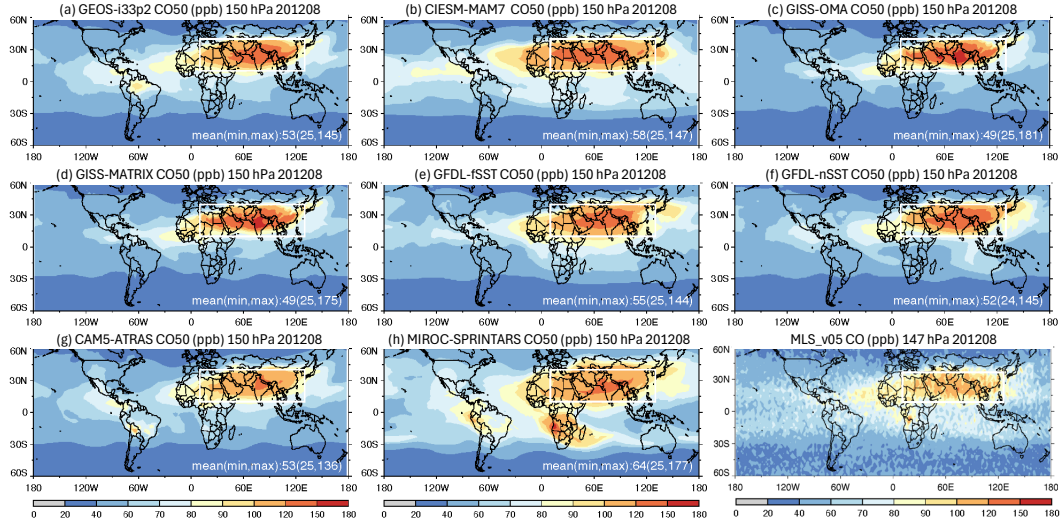

Figure 6: Same as Fig. 4 but for TR_{CO50}. The lower right panel shows CO at 147 hPa from Aura/MLS for reference.

Figure 7 shows the model simulated pressure-longitude vertical distributions of TR_{CO50} averaged over the 10°N–40°N latitude
250 band for August 2012. All models clearly display two major pollutant convective transport pathways over the ASM domain, one located at ~70–90°E over India and another at ~100–120°E over China. Convective transport of TR_{CO50} is also seen at locations west of 50°E over Middle East/eastern Africa region but this stem does not reach the upper troposphere except in CIESM-MAM7 (panel b). Convective transport over the North American monsoon region is also evident from the models but the TR_{CO50} concentrations are much lower owing to lower anthropogenic emissions there. In the middle to upper troposphere (500–120 hPa),
255 TR_{CO50} spreads both westward and eastward, reflecting large-scale upper-level divergence (e.g., Park et al., 2007) aided by transient eddy-shedding events (e.g., Pan et al., 2016; Honomichl and Pan, 2020).

Generally, the TR_{CO50} vertical pattern over the ASM region may be described as a "two-stem mushroom" shape. This pattern differs substantially from the AEC vertical cross-sections shown in Fig. 5, mainly because aerosols have much shorter lifetime (a few days), a greater variety of sources and compositions (e.g., pollution, smoke, dust, sea salt), and additional loss processes
260 through gravitational settling, dry deposition, and wet scavenging. These differences tend to confine aerosols, especially the coarse aerosol particles such as dust and sea salt, more tightly to their sources in the lower atmosphere.

Despite broad similarities in the transport features, the vertical extent and magnitude of TR_{CO50} over monsoon Asia still differs substantially across the models. For example, CAM5-ATRAS (panel g) and MIROC-SPRINTARS (panel h) lift TR_{CO50} more efficiently to the lower stratosphere with substantial concentrations above the tropopause, while TR_{CO50} is largely confined below
265 the tropopause in the other model simulations. The highest TR_{CO50} concentrations in the upper tropospheric ASMA region (300 hPa to the tropopause) produced by the two GISS model simulations (150–200 ppb, panels c and d) are 67% higher than the lowest concentrations reported by CAM5-ATRAS and MIROC-SPRINTARS (90–120 ppb, panels g and h). Yet, the mean TR_{CO50} concentrations at 150 hPa within the ASMA region (marked by white boxes in Fig. 6 and the grey horizontal lines in Fig. 7) are similar across the models, with a multi-model mean TR_{CO50} concentration of 105.2 ppb and a standard deviation of 3.5 ppb, leading

https://doi.org/10.5194/egusphere-2025-6257
Preprint. Discussion started: 14 January 2026

to a CV of 3.3% (Table 4). If the invariant background TR_{CO50} (25 ppb) from prescribed methane oxidation is removed, the multi-model mean drops to 80.2 ppb and the CV rises to 4.3%.

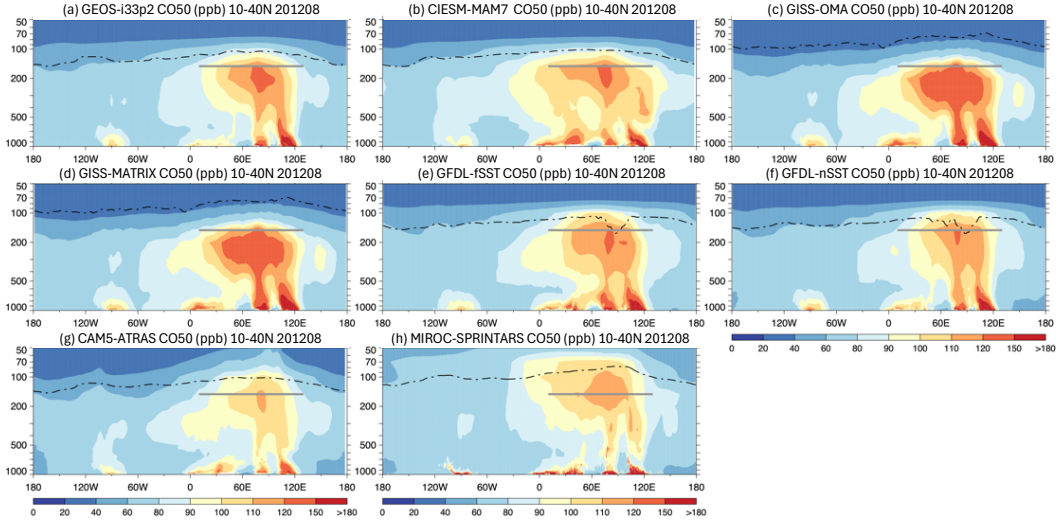

Figure 7: Same as Fig. 5 but for TR_{CO50}.

The features of TR_{CO50} from Fig. 6 and Fig. 7 suggest that the large inter-model differences in AEC in the 150 hPa ASMA region (CV = 79%) cannot be explained by differences in transport among the models (CV = 3%–4%). We next examine another important factor, wet removal, which is considered a major sink of atmospheric aerosols and is expected to play a significant role in inter-model differences in AEC.

3.3.2 Diagnosing inter-model differences in wet removal process

As introduced in Sect. 2.1, we use the model-incorporated pair of TR_{Rn}–TR_{Pb} tracers, specifically the ratio of TR_{Pb} to TR_{Rn} ($TR_{Pb/Rn}$), to diagnose the impact of inter-model differences in removal efficiencies on the upper tropospheric AEC. A smaller $TR_{Pb/Rn}$ indicates a higher removal efficiency, leading to a lower amount of aerosols in the upper troposphere. Although the TR_{Pb} production rates from prescribed TR_{Rn} decay are expected to be the same across the models globally, the spatial distributions of TR_{Pb} production may still differ because of inter- model differences in TR_{Rn} transport.

Figure 8 shows the longitude-pressure vertical cross sections of $TR_{Pb/Rn}$ averaged over the 10°N-40°N latitude band. The two GFDL simulations (panels e and f) produce the lowest $TR_{Pb/Rn}$ values in the vertical domain in Fig. 8, suggesting that the wet scavenging of aerosols is most efficient in this model. Similar results are also shown over the North American summer monsoon region and in the middle to the upper troposphere (200–400 hPa) for the entire 10°N-40°N band. By contrast, the CIESM-MAM7 model (panel b) shows the highest $TR_{Pb/Rn}$, indicating less efficient removal in this model. In the stratosphere, since TR_{Pb} experiences no wet removal while being continuously produced by the decay of TR_{Rn}, the $TR_{Pb/Rn}$ values should be much larger, as confirmed by most model simulations. However, the $TR_{Pb/Rn}$ values in the lower stratosphere remain at the tropospheric level in CAM5-ATRAS (panel g) and MIROC-SPRINTARS (panel h), which might be associated with the much deeper monsoon convection extending into the altitudes regarded as the lower stratosphere (shown in Fig. 7), leading to removal of TR_{Pb} similar to the behavior in the upper troposphere.

https://doi.org/10.5194/egusphere-2025-6257
Preprint. Discussion started: 14 January 2026

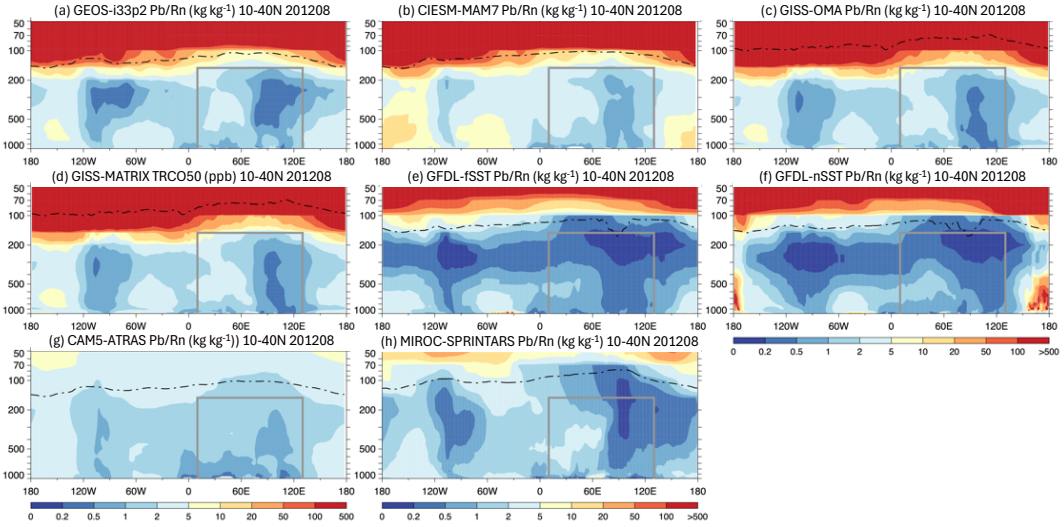

Figure 8: Same as Fig. 5 but for $TR_{Pb/Rn}$. The domain enclosed by the grey box is used to calculate the column integrated mean $TR_{Pb/Rn}$ values over ASMA region (see text for explanation).

To link the inter-model variability in AEC at 150 hPa ASMA region with the removal processes in the atmospheric column below, we compute the column-integrated, pressure-weighted mean $TR_{Pb/Rn}$ from surface to 150 hPa as an approximate indicator of the removal efficiency. Values of the mean $TR_{Pb/Rn}$ over the ASMA region (grey box in Fig. 8, averaged over 10°E–130°E) from individual models are listed in Table 4. The model CV in this metric is 36%, suggesting that the differences in wet scavenging among the models contribute more significantly to the inter-model diversity in AEC in the ASMA region than do differences in transport (CV = 3%–4%, Table 4).

3.3.3 Combined effect of transport and removal on inter-model differences in AEC

Another way to present the effects of transport and wet scavenging processes on aerosol amount in the upper tropospheric ASMA region is to examine correlations between model simulations of AEC and the individual or combined tracers, as shown in Fig. 9. The linear correlation coefficient (R) between AEC and TR_{CO50} is 0.37 and that between AEC and $TR_{Pb/Rn}$ is 0.62. With the two tracers together, R from the multivariable regression increases to 0.71, suggesting that differences in transport and the wet removal processes among these models can explain 50% (R^2 = 0.505) of the inter-model differences in AEC over the ASMA region, consistent with a simple summation of the CV values for the two tracers, i.e., 3% (TR_{CO50}) + 36% ($TR_{Pb/Rn}$) = 0.39%, which is roughly half of the 79% CV found for AEC.

The three models in group A (GEOS-i33p2, CIEMS-MAM7, and GISS-OMA, see Sect. 3.2), which simulate relatively higher values of AEC in the ASMA region (grey line in Fig. 9), have both relatively larger convective transport efficiencies (higher values in TR_{CO50}, red line) and smaller wet removal efficiencies (higher values in $TR_{Pb/Rn}$, blue line) compared to most models in group B (except GISS-MATRIX). The group B models exhibit either much lower convective transport efficiency (CAM5-ATRAS) or much higher wet removal efficiency (GFDL-fSST, GFDL-nSST, and MIROC-SPRINTARS) as possible explanations for producing lower AEC compared to group A. One notable exception is GISS-MATRIX, which produces TR_{CO50} and $TR_{Pb/Rn}$ values very similar to GISS-OMA but nearly three times smaller AEC than GISS-OMA. Such a large difference in AEC may arise mostly from the different representations of aerosols between these two versions of the GISS models: whereas GISS-OMA adopts a mass-based bulk aerosol model that assumes external mixtures of aerosol species, GISS-MATRIX uses a microphysical scheme that

https://doi.org/10.5194/egusphere-2025-6257
Preprint. Discussion started: 14 January 2026

tracks both aerosol mass and number concentrations and explicitly simulates the aerosol mixing state (Bauer et al., 2022). This difference in aerosol microphysics parameterization also affects aerosol lifetime, via different aerosol removal rates as a function of aerosol size.

The analysis in Sect. 3.2 and 3.3 uses the model simulations for August 2012 to examine the inter-model diversity of AEC in the upper tropospheric ASMA region, and to explain this diversity by the differences in transport efficiency and wet removal efficiency. Similar results are obtained for all other years in 2000-2018. Using CV as a matrix for measuring the inter-model differences, its value for AEC varies between 64% and 86% for August during the 19-year study period (mean = 77%), corresponding to the interannual variability of CV for TR_{CO50} between 2.5% and 7.7% (mean = 4.4%) and that for $TR_{Pb/Rn}$ between 34% and 38% (mean = 36%). Together, the inter-model differences in transport and wet removal can explain 44%-61% (mean = 52%) of the model diversity in AEC in the upper tropospheric ASMA region.

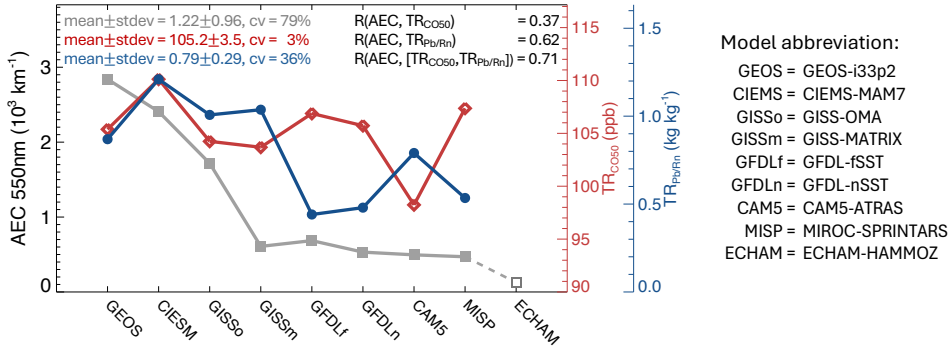

Figure 9: Model simulated mean values of AEC (grey), TR_{CO50} (red), and $TR_{Pb/Rn}$ (blue) in the ASM region in August 2012. The correlation coefficient R between AEC and TR_{CO50}, between AEC and $TR_{Pb/Rn}$, and between AEC and combined TR_{CO50} and $TR_{Pb/Rn}$ are shown on top right.

Other processes treated in each model, such as chemical formation of secondary aerosols (sulfate, nitrate, SOA), gravitational settling, particle size, and mass extinction efficiencies for aerosol species/sizes, also contribute to the differences in AEC. However, information from the model output submitted for the AeroCom UTLS experiment is not sufficient to quantitatively diagnose these contributions.

3.4 Two-decadal trend and interannual variability of non-volcanic aerosols in the upper tropospheric ASMA region

We use the multi-model means for each August from 2000 to 2018 at 150 hPa to represent the ensemble trend and interannual variability of non-volcanic aerosols in the upper tropospheric ASMA region. Figure 10 shows this time series (panel a) together with the corresponding ensemble means of convective transport, represented by TR_{CO50} at 150 hPa (panel b), and of aerosol removal within the atmospheric column, represented by $TR_{Pb/Rn}$ averaged from the surface to 150 hPa (panel c). For further context, changes in annual anthropogenic emissions of primary BC and OC and the secondary aerosol precursor gases of SO_2, NO_x, and NH_3 over Asia (5°N–50°N latitude, 65°E–130°E longitude) are also included (panel d), expressed as the percentage departure from the 19-year mean of each species.

The multi-model mean of AEC in the ASMA region at 150 hPa displays a statistically significant increasing trend from 2000 to 2018 at 0.014 10^3 km^{-1} yr^{-1}, equivalent to about 1.2 % yr^{-1} (trends and significance are shown in the bottom of each panel in Fig. 10), in contrast with the cases of the convective transport tracer TR_{CO50} and the removal tracer $TR_{Pb/Rn}$, neither of which shows any statistically significant trend. These results indicate that the variabilities in transport and removal processes over these two decades

https://doi.org/10.5194/egusphere-2025-6257
Preprint. Discussion started: 14 January 2026

do not contribute to the overall long-term increase in AEC within the ASMA region. On the other hand, the AEC trend is consistent with the increasing trends of anthropogenic emissions of primary aerosols and aerosol precursors in Asia (Fig. 10d), all of which shown a statistically significant increasing trends between 1.3% and 3.6% per year. This consistency can be shown in a more quantitative way: AEC does not correlate with either the transport tracer or wet removal tracer (R=0.08 and -0.14, respectively) but it correlates significantly with the surface anthropogenic emissions of all aerosol-related species (R = 0.73–0.82), mainly because both metrics have similar increasing trends. These results indicate that the increase in non-volcanic AEC in the ASM upper troposphere in recent decades has been determined by the growth of anthropogenic emissions in Asia.

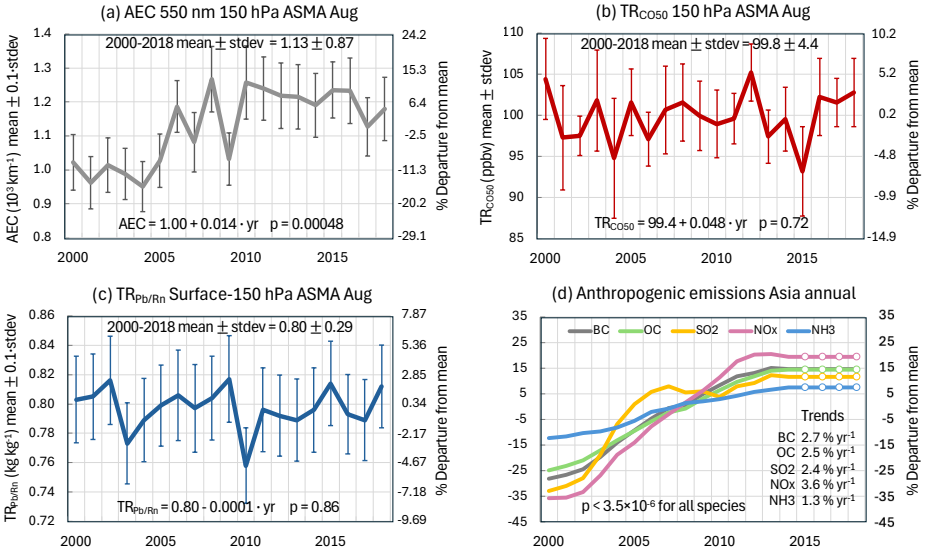

Figure 10: (a), (b), (c), left y-axis: Multi-model (excluding ECHAM6-HAMMOZ) means of AEC at 150 hPa, TR_{CO50} at 150 hPa, and $TR_{Pb/Rn}$ averaged between surface and 150 hPa, respectively, over the ASMA region in August from 2000 to 2018. The vertical lines are standard deviations of the model simulated values for the given year, which have been divided by 10 in (a) and (c) for clarity. Right y-axis: percentage departure of the values in individual years from the 19-year mean. The linear fitting of the trends is shown at the bottom of each panel together with significance of the trends ($p < 0.05$ from the student t-test is considered significant). (d): Annual CMIP6 anthropogenic emission trends of primary aerosols and secondary aerosol precursor gases in Asia from 2000 to 2018, expressed as percentage departure of annual amount from the 19-year mean (right y-axis). Anthropogenic emissions from 2015 to 2018 are kept the same as that in 2014 (shown in white circles). Correlation coefficients between AEC and other time series are listed in the text box below the panels.

We further examine the interannual variabilities of upper tropospheric AEC, TR_{CO50}, and $TR_{Pb/Rn}$ in the ASMA region using the multi-model ensemble means with the linear trend of AEC removed from the time series. To inspect how the interannual variabilities are related to large-scale climate or monsoon variabilities, we correlate the timeseries of detrended AEC, TR_{CO50}, and $TR_{Pb/Rn}$ with the Multivariate El Niño/Southern Oscillation (ENSO) Index version 2 (MEI.v2) and two Asian summer monsoon indices, the East Asian Summer Monsoon Index (EASMI) and the South Asian Summer Monsoon Index (SASMI). Table 5 provides brief descriptions of these indices.

As shown in Fig. 11, the detrended AEC, TR_{CO50}, and $TR_{Pb/Rn}$ exhibit moderate correlations with MEI.v2, with both AEC and TR_{CO50} negatively correlated (R = -0.41 and -0.42, respectively) but $TR_{Pb/Rn}$ positively correlated with MEI.v2 (R = 0.68). These relationships imply that during years with negative MEI (e.g., La Niña conditions), convective transport tends to be more efficient while wet removal tends to be less efficient over the ASM region, leading to higher AEC values in the upper troposphere compared

https://doi.org/10.5194/egusphere-2025-6257
Preprint. Discussion started: 14 January 2026

to years with positive MEI.v2 (e.g., El Niño conditions). By contrast, variations in AEC and the two tracers in the ASMA regions show low correlations with the two wind-based Asian summer monsoon indices, SASMI and EASMI (R = -0.16 and -0.29, respectively; Figures not shown).

The multi-model ensemble results presented in this section suggest that the non-volcanic AEC trend in the upper tropospheric ASMA region corresponds to anthropogenic emission trends in Asia, while interannual variability in AEC appears to be linked to climate variability represented by MEI.v2.

Table 5. Climate and Asian summer monsoon indices.

	MEI.v2	SASMI	EASMI
Definition	Bimonthly overlapping leading combined Empirical Orthogonal Function of five variables (sea level pressure, sea surface temperature, zonal and meridional components of the surface wind, and outgoing longwave radiation) over the tropical Pacific basin (30°S–30°N and 100°E-70°W)	An area-averaged dynamical normalized seasonality index (JJA) based on intensity of the normalized wind fields at 850 hPa within the South Asian domain (5°N–22.5°N, 35°E–97.5°E)	An area-averaged dynamical normalized seasonality index (JJA) based on intensity of the normalized wind fields at 850 hPa within the East Asian monsoon domain (10°N–40°N, 110°E–140°E)
References	Zhang et al., 2019	Li and Zeng, 2005	Li and Zeng, 2005
Weblink	https://psl.noaa.gov/enso/mei	http://lijianping.cn/dct/page/65576	http://lijianping.cn/dct/page/65577

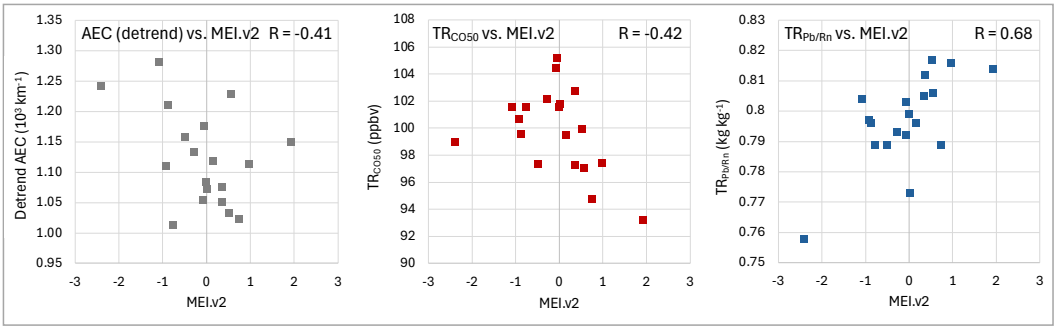

Figure 11: Scatter plots of correlations between MEI.v2 and the detrended AEC (left), TR_{CO50} (middle), and $TR_{Pb/Rn}$ (right) over the ASMA region for each August in 2000–2018.

4 Discussion

In this section, we discuss several modeling and evaluation issues encountered in the preceding analysis of UTLS aerosols, to shed some lights on how to advance future synergistic efforts.

Inter-model differences in AEC: The multi-model simulated non-volcanic AEC in the summertime upper troposphere show considerable differences (e.g., Fig. 4–6), with an inter-model CV across the eight models ranging from 64% to 84% for each August during 2000–2018 in the ASMA region. Based on the behavior of the common transport tracer TR_{CO50} and removal tracer $TR_{Pb/Rn}$ implemented in all models, the inter-model variability in aerosol removal processes is much larger (CV = 34%–38%) than that in transport (CV = 2%–8%), indicating that wet removal bears greater responsibility for the inter-model differences in AEC. Other factors, such as chemical processes for secondary aerosol formation or aerosol microphysical and optical properties, are expected to be important as well in determining AEC; however, as stated in Sect. 3.3, evaluation of these differences would require additional outputs. On the other hand, the shortage of observable metrics for diagnosing aerosol processes greatly limits the use of observations to improve or constrain model simulations. Moreover, differences in the simulated volcanic AEC in the BASE

https://doi.org/10.5194/egusphere-2025-6257
Preprint. Discussion started: 14 January 2026

experiment (Fig. 2 and 3) suggest that significant challenges remain in how these models represent volcanic aerosols. Potential sources of differences include implementations of volcanic emissions, injection heights, chemical transformation, and losses, even though all models should have prescribed the same volcanic emission and plume height data. Clearly, considerable effort is needed in the modeling community to improve the volcanic aerosol simulation capabilities for broader applications. Lastly, the inclusion of the "background" sulfate aerosols from OCS oxidation is necessary to accurately simulate the amount of stratospheric aerosols, as these could be the major contributor to total aerosol loading above the tropopause during volcanically quiescent periods. Most models that participated in the UTLS model experiment did not consider this process, hampering meaningful assessment of the lower stratospheric aerosol composition, variability, and trend.

Diagnostic tracers: In this model experiment, eight out of nine participating models have implemented the requested transport and removal tracers, enabling a quantitative diagnosis of the causes of inter-model differences in aerosol simulations. As demonstrated in Sect. 3.3, these tracers provide valuable information on the characteristics of advection, convection and aerosol removal efficiency, facilitating more quantitative assessment of inter-model differences beyond the qualitative or suggestive attributions seen in previous studies. Still, several caveats apply when interpreting the results. For TR_{CO50}, a major advantage is that the emissions of CO from anthropogenic, biomass burning, and biogenic sources are usually co-located with emissions of fine-mode aerosols and their precursors. In addition, the abundance of CO observations from satellite and in-situ platforms can help evaluate the model representations of the transport pathways from those sources to the upper troposphere and lower stratosphere. However, the longer atmospheric lifetime of TR_{CO50} (50 days in this study) relative to aerosols (roughly one order of magnitude less) and the relatively large magnitude of the background TR_{CO50} source produce a narrower spread across the models than that found for aerosols. In addition, this tracer is not suitable for tracking aerosols emitted from deserts, oceans, or other places that have entirely different source locations as CO. For the removal tracer $TR_{Pb/Rn}$, the differences among models may be compounded by transport patterns of TR_{Rn}, such that the inter-model differences of $TR_{Pb/Rn}$ may not arise entirely from differences in wet removal. As we discussed earlier, additional diagnostics tracers for secondary aerosol production and aerosol microphysical properties (particle size, mass extinction efficiency, hygroscopic properties, etc.) are needed to better understand the inter-model differences.

Tropopause height: As shown in Fig. 5, 7, and 8, the August mean tropopause heights differ by tens of hPa across the models. The GISS models show the highest tropopause height while the GFDL model plunges to lower altitudes over the ASM region, possibly due to the differences in how the tropopause height is diagnosed. The tropopause height can be defined in several different ways, including a thermal definition based on the temperature lapse rate (World Meteorological Organization, 1957), multiple dynamical definitions using various potential vorticity thresholds (e.g., Hoinka, 1998), and composition-based definitions based on the sharpness of the trace gas gradients such as ozone or water vapor (e.g., Shepherd, 2002). Although the tropopause height is a diagnostic quantity that does not influence the prognostic physical processes evaluated in this study, its vertical placement affects the quantitative assessments of stratosphere-troposphere exchange, composition in the lower stratosphere, and stratospheric column integrals such as stratospheric aerosol optical depth, among other features (e.g., Millán et al., 2024). Users engaged in those studies should thus be mindful of differences in defined and simulated tropopause heights.

Evaluation of model simulated UTLS aerosols with satellite data: Vertically resolved satellite aerosol data are mostly available from active sensors or limb scatter instruments that provide aerosol extinction or backscatter data. As mentioned in Sect. 3.1, retrievals using these instruments to target the upper troposphere and tropopause regions are subject to larger uncertainties because of the difficulties in separating aerosols from ice clouds. These uncertainties impede quantitative model evaluation. Aircraft measurements of aerosols in the upper troposphere, particularly those collected in and around ASMA, such as StratoClim in summer 2017 over Nepal/India (e.g., Appel et al., 2022; Mahnke et al., 2021) and ACCLIP in summer over the western North

https://doi.org/10.5194/egusphere-2025-6257
Preprint. Discussion started: 14 January 2026

Pacific (Pan et al., 2025), will be extremely valuable for evaluating model simulations of aerosols and related species in this regions. However, balanced against their precision and accuracy, aircraft data have limited coverage in space and time. Accordingly, harmonizing the use of remote sensing and in-situ data for model evaluation requires coordinated efforts toward planning and execution in both the modeling and measurement communities.

5 Conclusions

This study presents results from the AeroCom Phase-III UTLS model experiment designed to investigate aerosols in the upper troposphere associated with Asian summer monsoon dynamics and assess their two-decadal trend and interannual variability. Although all participating models used identical prescribed anthropogenic, biomass burning, and volcanic emissions, substantial differences emerge in the simulated AEC in the UTLS. A major issue stems from inconsistent implementations of volcanic aerosols, which leads to irreconcilable differences in volcanic aerosol extinction across models. Our analysis therefore focuses on non-volcanic aerosols, which are mostly influenced by the ASM dynamics, simulated by the nine participating global models. The key findings are summarized below.

There are significant differences in model-simulated AEC in the upper troposphere over the ASMA region despite identical emission inputs. A case study for August 2012 has revealed large AEC disparities among models, with a maximum-to-minimum ratio exceeding a factor of 20. Using two diagnostic tracers, TR_{CO50} for transport and $TR_{Pb/Rn}$ for wet removal, in eight models, we attribute a substantial fraction of the inter-model differences in AEC to specific processes. All model simulations exhibited the characteristics of "two-stem mushroom" vertical structure of TR_{CO50}, reflecting strong ASM convection that lifts surface pollutants in Asia into the upper troposphere, where they are then distributed horizontally by the upper-level anticyclonic circulation. Inter-model variability in TR_{CO50} is small in the upper tropospheric ASMA region (CV = 3%–4%), far lower than the variability in AEC (CV = 79%). By contrast, $TR_{Pb/Rn}$, which represents aerosol wet removal efficiency, shows much larger inter-model variability (CV = 36%) than transport. Thus, wet removal differences play a greater role in generating the inter-model spread in AEC in the upper troposphere than do differences in transport. This behavior is consistent across all years from 2000 to 2018 with CV = 64%–86% for AEC, 2%–8% for TR_{CO50}, and 34%–38% for $TR_{Pb/Rn}$. Together, transport and wet removal processes account for roughly half (44%–56%) of the AEC diversity across models. Additional factors, such as secondary aerosol formation and aerosol microphysical or optical properties, may also contribute, warranting further investigation with appropriate diagnostic tools.

Using multi-model ensemble means at 150 hPa over the ASMA region, we find a statistically significant positive trend in AEC during 2000-2018 (0.014 10^3 km^{-1} or 1.2% yr^{-1}), despite the lack of any significant trend in either transport (represented by TR_{CO50}) or wet removal (represented by $TR_{Pb/Rn}$). The AEC trend aligns closely with increasing anthropogenic emission of primary aerosols and precursor gases in Asia over the same period, all showing statistically significant positive trends (1.3%–3.6% yr^{-1}) and strong correlations with AEC (R = 0.73–0.82). Meanwhile, interannual variations in detrended AEC, TR_{CO50}, and $TR_{Pb/Rn}$ are correlated with the major climate variability represented by the index MEI.v2 While both AEC and TR_{CO50} exhibit moderate negative correlations (R = -0.41 and -0.42, respectively), $TR_{Pb/Rn}$ shows a positive correlation (R = 0.68) with MEI.v2. These relationships suggest that climate variability modulates ASM transport and wet removal processes: AEC tends to be higher during La Niña years (negative MEI.v2) due to generally stronger upward transport and weaker wet removal, and vice versa during El Niño years (positive MEI.v2).

The present study yields several key recommendations:

1. **Improve observational constraints for model simulations of aerosols in the upper troposphere.** Satellite retrievals of AEC remain challenging due to the difficulties of separating relatively weak aerosol signals from the frequent

https://doi.org/10.5194/egusphere-2025-6257
Preprint. Discussion started: 14 January 2026

occurrence of ice clouds in the upper troposphere. Better integration of satellite observations with coordinated aircraft campaigns is essential for constraining aerosol processes simulated by models.

2. **Expand diagnostic tracers for process attribution.** The pollutant transport tracer and wet removal tracers used in this study have proven effective for quantitatively diagnosing inter-model differences and attributing the cause of inter-model differences. They can also be applied to evaluate interannual variabilities within individual models or benchmark improvements across model versions. Additional diagnostics tools for chemical transformation and aerosol microphysical properties would be highly valuable, though standardizing them for multi-model applications will require community effort.
3. **Advance UTLS aerosol simulation capabilities in the AeroCom modeling community.** Greater community attention is needed to improve model simulation of aerosols in the UTLS, particularly with respect to representations of volcanic aerosol and background sulfate aerosol, both of which strongly influence stratospheric aerosol burdens.

Data availability

The datasets used in this work are publicly accessible. The AeroCom UTLS model output is stored in the AeroCom repository, which can be accessed on request, as described at https://aerocom.met.no/data/. Aerosol extinction retrieved from SCIAMACHY observations at the University of Bremen is publicly available at https://www.iup.uni-bremen.de/DataRequest/. The OSIRIS data can be downloaded from https://arg.usask.ca/docs/osiris_v7/. Aerosol extinction retrieved from OMPS LP can be accessed from https://avdc.gsfc.nasa.gov/pub/tmp/OMPS_aer/aer_gridded/. CALIPSO Lidar Level 3 Stratospheric Aerosol Profiles data available at https://doi.org/10.5067/CALIOP/CALIPSO/LID_L3_STRATOSPHERIC_APRO-STANDARD-V1-00/.

Author contributions

MC conceived this project and designed the model experiment in collaboration with HB and XP. HB, SB, PG, ZG, SF, AL, HM, YP, KT, TT, and JSW contributed model simulations. JPB, GT, JK, LR, AR, AB, and CA provided the L3 satellite aerosol data. QT helped with satellite CO data. MC conducted the analysis, wrote the initial draft, and finalized the manuscript with contributions from all coauthors. JSW provided thorough editing on the manuscript.

Competing interests

Two coauthors are members of the editorial board of Atmospheric Chemistry and Physics. Others declare that they have no conflict of interest.

Acknowledgements

We thank the Norwegian Meteorological Institute AeroCom team (Michael Schulz, Anna Benedictow, et al.) for supporting the AeroCom model experiment, providing AeroCom model repository, and facilitating data access; JPL MLS team for satellite CO data; Simon Carn for providing volcanic SO_2 dataset; CEDS and GFED teams for anthropogenic and biomass burning emission datasets; and the IGAC/APARC ACAM community for collaboration. Authors at GSFC (MC, HB, and XP) and GISS (KT, SB) also acknowledge their respective organizations (the Atmospheric Chemistry and Dynamic (ACD) Laboratory and Global

https://doi.org/10.5194/egusphere-2025-6257
Preprint. Discussion started: 14 January 2026

Modeling and Assimilation Office (GMAO) at GSFC, and climate modeling at GISS, respectively) for model infrastructure, software resources, and IT support, and the NASA High-end computing (HEC) facilities through the NASA Center for Climate Simulations (NCCS) for computational resources.

Financial support

MC, HB, QT, and XP were supported by NASA Earth Science Programs of Aura ST, ACMAP, ISFM, and MAP. JSW, YP and ZG were supported by the National Natural Science Foundation of China (Grants 42275053, 42175096, and 42205085), the Open Fund for the Ministry of Education Key Laboratory for Earth System Modeling (2023), and the National Key Scientific and Technological Infrastructure project "Earth System Numerical Simulation Facility" (EarthLab). HM was supported by the Ministry of Education, Culture, Sports, Science, and Technology (MEXT) and the Japan Society for the Promotion of Science (JSPS) through KAKENHI Grants (JP23K18519 and JP23K24976), the MEXT Arctic Challenge for Sustainability II (ArCS II; JPMXD1420318865) and 3 (ArCS-3; JPMXD1720251001) Projects, and the Environment Research and Technology Development Fund 2-2301 (JPMEERF20232001) of the Environmental Restoration and Conservation Agency. KT and SB were supported by NASA Modeling, Analysis and Prediction program (MAP). TT was supported by the Environment Research and Technology Development Fund S-20 (JPMEERF21S12010) of the Environmental Restoration and Conservation Agency provided by the Ministry of Environment of Japan, and the NEC SX supercomputer system of the National Institute for Environmental Studies of Japan. JPB, AR and CA were funded in part by the State and University of Bremen, ESA (project CREST) and the German Research Foundation (DFG) Research Unit VolImpact (FOR 2820).

References

Appel, O. Köllner, F., Dragoneas, A., Hünig, A., Molleker, S., Schlager, H., et al.: Chemical analysis of the Asian tropopause aerosol layer (ATAL) with emphasis on secondary aerosol particles using aircraft-based in situ aerosol mass spectrometry, Atmos. Chem. Phys., 22, 13607–13630. https://doi.org/10.5194/acp-22-13607-2022, 2022.

Balkanski, Y. J., D. Jacob, G. M. Gardner, W. C. Graustein, and K. K. Turekian: Transport and residence times of tropospheric aerosols inferred from a global three-dimensional simulation of 210Pb, J. Geosphys. Res., 98, 20571-20586, https://doi.org/10.1029/93JD02456, 1993.

Bauer, S. E., Wright, D. L., Koch, D., Lewis, E. R., McGraw, R., Chang, L.-S., et al.: MATRIX (Multiconfiguration Aerosol TRacker of mIXing state): an aerosol microphysical module for global atmospheric models, Atmos. Chem. Phys., 8, 6003–6035, www.atmos-chem-phys.net/8/6003/2008/, 2008.

Bauer, S. E., Tsigaridis, K., Faluvegi, G., Nazarenko, L., Miller, R. L., Kelley, M., & Schmidt, G.: The turning point of the aerosol era. Journal of Advances in Modeling Earth Systems, 14, e2022MS003070. https://doi.org/10.1029/2022MS003070, 2022.

Bovensmann, H., Burrows, J., Buchwitz, M., Frerick, J., Noël, S., Rozanov, V., Chance, K., and Goede, A.: SCIAMACHY: mission objectives and measurement modes, J. Atmos. Sci., 56, 127–150, https://doi.org/10.1175/1520-0469(1999)056<0127:SMOAMM>2.0.CO;2, 1999.

Bourassa, A. E., Rieger, L. A., Lloyd, N. D., and Degenstein, D. A.: Odin-OSIRIS stratospheric aerosol data product and SAGE III intercomparison, Atmos. Chem. Phys., 12, 605–614, https://doi.org/10.5194/acp-12-605-2012, 2012.

Burrows, J. P., Hölzle, E., Goede, A. P. H., Visser, H., and Fricke, W.: SCIAMACHY - Scanning Imaging Absorption Spectrometer for Atmospheric Chartography, Acta Astronautica, 35(7), 445-451, https://doi.org/10.1016/0094-5765(94)00278-T, 1995.

https://doi.org/10.5194/egusphere-2025-6257
Preprint. Discussion started: 14 January 2026

Chin, M., Diehl, T., Dubovik, O., Eck, T. F., Holben, B. N., Sinyuk, A., and Streets, D. G.: Light absorption by pollution, dust, and biomass burning aerosols: a global model study and evaluation with AERONET measurements, ANGEO, 27, 3439–3464, https://doi.org/10.5194/angeo-27-3439-2009, 2009.

Colarco, P., da Silva, A., Chin, M., and Diehl, T.: Online simulations of global aerosol distributions in the NASA GEOS-4 model and comparisons to satellite and ground-based aerosol optical depth, J. Geophys. Res.-Atmos., 115, D14207, https://doi.org/10.1029/2009JD012820, 2010.

Carn, S. A., K. Yang, A. J. Prata, and N. A. Krotkov: Extending the long-term record of volcanic SO_2 emissions with the Ozone Mapping and Profiler Suite nadir mapper, Geophys. Res. Lett., 42, 925-932. https://doi.org/10.1002/2014GL062437, 2015.

Carn, S. A., V. E. Fioletov, C. A. McLinden, C. Li, and N. A. Krotkov: A decade of global volcanic SO_2 emissions measured from space, Sci. Reports, https://doi,org/10.1038/srep44095, 2017.

Fadnavis, S., Kalita, G., Kumar, K. R., Gasparini, B., & Li, J.-L. F.: Potential impact of carbonaceous aerosol on the upper troposphere and lower stratosphere (UTLS) and precipitation during Asian summer monsoon in a global model simulation. Atmos. Chem. Phys., 17, 11637-11654. https://doi.org/10.5194/acp-17-11637-2017, 2017.

Fadnavis, S., Roy, C., Chattopadhyay, C., Sioris, C. E., Rap, A., Müller, R., et al.: Transport of trace gases via eddy shedding from the Asian summer monsoon anticyclone and associated impacts on ozone heating rates, Atmos. Chem. Phys., 18, 11493-11506, https://doi.org/10.5194/acp-18-11493-2018, 2018.

Fadnavis, S., Müller, R., Kalita, G., Rowlinson, M., Rap, A., Li, J.-L. F., et al.: The impact of recent changes in Asian anthropogenic emissions of SO_2 on sulfate loading in the upper troposphere and lower stratosphere and the associated radiative changes. Atmos. Chem. Phys., 19, 9989-10008. https://doi.org/10.5194/acp-19-9989-2019, 2019.

Gao, J., Huang, Y., Peng, Y. and Wright, J. S.: Aerosol Effects on Clear-Sky Shortwave Heating in the Asian Monsoon Tropopause Layer, J. Geophys. Res. Atmospheres 128, e2022JD036956, https://doi.org/10.1029/2022JD036956, 2023.

Gettelman, A., Kinnison, D. E., Dunkerton, T. J., and Brasseur, G. P.: Impact of monsoon circulations on the upper troposphere and lower stratosphere, J. Geophys. Res., 109, D22101, https://doi:10.1029/2004JD004878, 2004.

Hanumanthu, S., Vogel, B., Müller, R., Brunamonti, S., Fadnavis, S., Li, D., et al.: Strong day-to-day variability of the Asian TropopauseAerosol Layer (ATAL) in August 2016 at the Himalayan foothills. Atmospheric Chemistry and Physics, 20(22), 14273–14302. https://doi.org/10.5194/acp-20-14273-2020, 2020.

Hoesly R. M., Smith, S. J., Feng, L., Klimont, Z., Janssens-Maenhout, G., Pitkanenet. T., et al.: Historical (1750–2014) anthropogenic emissions of reactive gases and aerosols from the Community Emissions Data System (CEDS), Geosci. Model Dev., 11, 369–408, https://doi.org/10.5194/gmd-11-369-2018, 2018.

Hoinka, K. P.: Statistics of the global tropopause pressure, Mon. Weather Rev., 126, 3303-3325, 1998.

Honomichl, S. B., and Pan, L. L.: Transport from the Asian summer monsoon anticyclone over the western Pacific, J. Geophys. Res.: Atmospheres, 125, e2019JD032094, https://doi.org/10.1029/2019JD032094, 2020.

Jiang, J. H., Livesey, N. J., Su, H., Neary, L., McConnell, J. C., and Richards, N. A. D.: Connectin surface emissions, convective uplifting, and long-range transport of carbon monoxide in the upper troposphere: New observations from the Aura Microwave Limb Souder, Geophys. Res. Lett., 34, L18812, https://doi.org/10.1029/2007GL030638, 2007.

Kar, J., Bremer, H., Drummond, J. R., Rochon, Y. J., Jones, D. B. A., Nichitiu, F., Zou, J., Liu, J., Gille, J. C., Edwards, D. P., Deeter, M. N., Francis, G., Ziskin, D., and Warner, J.: Evidence of vertical transport of carbon monoxide from Measurements of Pollution in the Troposphere, Geophys. Res. Lett., 31, L23105, https://doi.org/10.1029/2004GL021128, 2004.

https://doi.org/10.5194/egusphere-2025-6257
Preprint. Discussion started: 14 January 2026

Kar, J., Lee, K.-P., Vaughan, M. A., Tackett, J. L., Trepte, C. R., Winker, D. M., Lucker, P. L., and Getzewich, B. J.: CALIPSO Level 3 stratospheric aerosol profile product: Version 1.00 algorithm description and initial assessment, Atmos. Meas. Tech., 12, 6173–6191, https://doi.org/10.5194/amt-12-6173-2019, 2019.

Koch, D., Schmidt, G. A., and Field, C. V.: Sulfur, sea salt, and radionuclide aerosols in GISS ModelE, J. Geophys. Res.-Atmos., 111, D06206, https://doi.org/10.1029/2004JD005550, 2006.

Kremser, S., Thomason, L. W., von Hobe, M., Hermann, M., Deshler, T., Timmreck. C., et al.: Stratospheric aerosol—observations, processes, and impact on climate, Rev. Geophys., 54, 278–335, https://doi.org/10.1002/2015RG000511, 2016.

Langille, J., Rieger, L. A., Blanchard, Y., Blanchet, J.-P., Bourassa, A., Degenstein, D., et al.: A high-latitude aerosols, water vapour and clouds mission: concept, scientific objectives and data products, BAMS, https://doi.org/10.1175/BAMS-D-23-0309.1, 2025.

Lau, W. K. M., Yuan, C., and Li, Z.: Origin, Maintenance and Variability of the Asian Tropopause Aerosol Layer (ATAL): The Roles of Monsoon Dynamics, Sci. Report, 8, 3960, https://doi:10.1038/s41598-018-22267-z, 2018.

Legras, B., and Bucci, S.: Confinement of air in the Asian monsoon anticyclone and pathways of convective air to the stratosphere during the summer season, Atmos. Chem. Phys., 20, 11045–11064, https://doi.org/10.5194/acp-20-11045-2020, 2020.

Li, J. and Zeng, Q. C: A unified monsoon index. Geophys. Res. Lett., 29(8), 1274, https://doi.org/10.1029/2001GL013874, 2002.

Li, Q. B., Jiang, J. H., Wu, D. L., Read, W. G., Livesey, N. J., Waters, J. W., et al.: Convective outflow of south Asian pollution: A global CTM simulation compared with EOS MLS observations, Geophys. Res. Lett., 32, L14826, https://doi.org/10.1029/2005GL022762, 2005.

Liang, Q., Newman, P. A., Fleming, E. L., Lait, L. R., Atlas, E., Pan, L., et al.: Asian summer monsoon anticyclone – the primary entryway for chlorinated very-short-lived substances to the stratosphere, Geophys. Res. Lett., 52, e2024GL110248, https://doi.org/10.1029/2024GL110248, 2025.

Lin, Y., Huang, X., Liang, Y., Qin, Y., Xu, S., Huang, W., et al.: Community Integrated Earth System Model (CIESM): Description and Evaluation, J. Adv. Modeling Earth Sys., 12, e2019MS002036. https://doi.org/10.1029/2019MS002036, 2020.

Liu, H., Jacob, D., Bey, I., and Yantosca, B. M.: Constraints from 210Pb and 7Be on wet deposition and transport in a global three-dimensional chemical tracer model driven by assimilated meteorological fields, J. Geophys. Res., 106, 12109-12128, https://doi.org/10.1029/2000JD900839, 2001.

Ma, J., Brühl, C., He, Q., Steil, B., Karydis, V. A., Klingmüller, K., et al.: Modeling the aerosol chemical composition of the tropopause over the Tibetan Plateau during the Asian summer monsoon. Atmospheric Chemistry and Physics, 19(17), 11587–11612. https://doi.org/10.5194/acp-19-11587-2019, 2019.

Mahnke, C., Weigel, R., Cairo, F., Vernier, J.-P., Afchine, A., Krämer, M., et al.: The Asian tropopause aerosol layer within the 2017monsoon anticyclone: Microphysical properties derived from aircraft-borne in situ measurements. Atmospheric Chemistry and Physics,21(19), 15259–15282. https://doi.org/10.5194/acp-21-15259-2021, 2021.

Malinina, E., Rozanov, A., Vountas, M., and Burrows, J.: Stratospheric aerosol extinction coefficient, available at: http://www.iup.uni-bremen.de/scia-arc/, last access: 31 May 2018.

Matsui, H.: Development of a global aerosol model using a two-dimensional sectional method: 1. Model design, J. Adv. Model. Earth Sy., 9, 1921-1947, https://doi.org/10.1002/2017MS000936, 2017.

Matsui, H. and Mahowald, N.: Development of a global aerosol model using a two-dimensional sectional method: 2. Evaluation and sensitivity simulations, J. Adv. Model. Earth Sy.s, 9, 1887-1920, https://doi.org/10.1002/2017MS000937, 2017.

https://doi.org/10.5194/egusphere-2025-6257
Preprint. Discussion started: 14 January 2026

Millán, L. F. Hoor, P., Hegglin M., Manney, G. L., Boenisch, H., Jeffery, P., et al.: Exploring ozone variability in the upper troposphere and lower stratosphere using dynamical coordinates. Atmos. Chem. Phys. 24, 7927–7959, https://doi.org/10.5194/acp-24-7927-2024, 2024.

Noël, S., Bramstedt, K., Rozanov, A., Malinina, E., Bovensmann, H., and Burrows, J. P.: Stratospheric aerosol extinction profiles from SCIAMACHY solar occultation, Atmos. Meas. Tech., 13, 5643–5666, https://doi.org/10.5194/amt-13-5643-2020, 2020.

Pan, L. L., Honomichl, S. B., Kinnison, D. E., Abalos, M., Randel, W. J., Bergman, J. W., and Bian, J.: Transport of chemical tracers from the boundary layer to stratosphere associated with the dynamics of the Asian summer monsoon. Journal of Geophysical Research: Atmospheres, 121, 14159–14174, https://doi.org/10.1002/2016JD025616, 2016.

Pan, L., Atlas, E. L., Newman, P. A., Thornberry, T., Jucks, K., Toon, O., et al.: The Asian Summer Monsoon Chemical and Climate Impact Project (ACCLIP): An Overview. ESS Open Archive, July 24, https://doi.org/10.22541/essoar.175337658.88281458/v1, 2025.

Park, M., Randel, W. J., Gettelman, A., Massie, S. T., & Jiang, J. H.: Transport above the Asian summer monsoon anticyclone inferred from Aura Microwave Limb Sounder tracers. Journal of Geophysical Research, 112(D16), D16309. https://doi.org/10.1029/2006jd008294, 2007.

Park, M., Randel, W. J., Emmons, L. K., and Livesey, N. J.: Transport pathways of carbon monoxide in the Asian summer monsoon diagnosed from Model of Ozone and Related Tracers (MOZART), J. Geophys. Res., 114, D08303, https://doi:10.1029/2008JD010621, 2009.

Ploeger, F., Konopka, P., Walker, K., and Riese, M.: Quantifying pollution transport from the Asian monsoon anticyclone into the lower stratosphere. Atmos Chem Phys 17, 7055–7066, https://doi.org/10.5194/acp-17-7055-2017, 2017.

Popovic, J. M., and Plumb, R. A.: Eddy shedding from the upper-tropospheric Asian monsoon anticyclone, J. Atmos. Sci., 58, 93–104, https://doi.org/10.1175/1520-0469(2001)058<0093:ESFTUT>2.0.CO;2, 2001.

Randel, W. J., and Park, M.: Deep convective influence on the Asian summer monsoon anticyclone and associated tracer variability observed with Atmospheric Infrared Sounder (AIRS), J. Geosphys. Res. Atmospheres, 111, D12314, https://doi:10.1029/2005JD006490, 2006.

Randel, W. J., Park, M., Emmons, L., Kinnison, D., Bernath, P., Walker, K. A., Boone, C., and Pumphrey, H.: Asian Monsoon Transport of Pollution to the Stratosphere, Science, 328, 611-613, https://doi.org/10.1126/science.1182274, 2010.

Rieger, L. A., Bourassa, A. E., and Degenstein, D. A.: Merging the OSIRIS and SAGE II stratospheric aerosol records, J. Geophys. Res. Atmos., 120, https://doi:10.1002/2015JD023133, 2015.

Rieger, L. A., Zawada, D. J., Bourassa, A. E., and Degenstein, D. A.: A multiwavelength retrieval approach for improved OSIRIS aerosol extinction retrievals, J. Geophys. Res. Atmospheres, 124, 7286–7307. https://doi.org/10.1029/2018JD029897, 2019.

Santee, M. L., Manney, G. L., Livesey, N. J., Schwartz, M. J., Neu, J. L., and Read, W. G.: A comprehensive overview of the climatological composition of the Asian summer monsoon anticyclone based on 10 years of Aura Microwave Limb Sounder measurements, J. Geophys. Res. Atmos., 122, 5491–5514, https://doi.org/10.1002/2016JD026408, 2017.

Schultz, M. G., Stadtler, S., Schröder, S., Taraborrelli, D., Franco, B., Krefting, J., et al.: The chemistry–climate model ECHAM6.3-HAM2.3-MOZ1.0, Geosci. Model Devel., 11, 1695-1723, https://doi.org/10.5194/gmd-11-1695-2018, 2018.

Shepherd, T. G., Issues of stratosphere-troposphere coupling, J. Met. Soc. Japan, 80, 769-792, 2002.

Soulie, A., Granier, C., Darras, S., Zilbermann, N., Doumbia, T., Guevara, M., et al.: Global anthropogenic emissions (CAMS-GLOB-ANT) for the Copernicus Atmosphere Monitoring Service simulations of air quality forecasts and reanalyses, Earth Syst. Sci. Data, 16, 2261–2279, https://doi.org/10.5194/essd-16-2261-2024, 2024.

https://doi.org/10.5194/egusphere-2025-6257
Preprint. Discussion started: 14 January 2026

Taha, G., Loughman, R., Zhu, T., Thomason, L., Kar, J., and Rieger. L: OMPS LP Version 2.0 multi-wavelength aerosol extinction coefficient retrieval algorithm, Atmos. Meas. Tech., 14, 1015–1036, https://doi.org/10.5194/amt-14-1015-2021, 2021.

Takemura, T., Nozawa, T., Emori, S., Nakajima, T. Y., and Nakajima, T.: Simulation of climate response to aerosol direct and indirect effects with aerosol transport-radiation model, J. Geophys. Res.-Atmos., 110, D02202, https://doi.org/10.1029/2004JD005029, 2005.

Tsigaridis, K., Koch, D., and Menon, S.: Uncertainties and importance of sea spray composition on aerosol direct and indirect effects, J. Geophys. Res.-Atmos., 118, 220-235, https://doi.org/10.1029/2012JD018165, 2013.

Ungermann, J., Ern, M., Kaufmann, M., Müller, R., Spang, R., Ploeger, F., Vogel, B., and Riese, M.: Observations of PAN and its confinement in the Asian summer monsoon anticyclone in high spatial resolution, Atmos. Chem. Phys., 16, 8389–8403, https://doi.org/10.5194/acp-16-8389-2016, 2016.

van der Werf, G. R., Randerson, J. T., Giglio, L., van Leeuwen, T. T., Chen, Y., Rogers, B. M. et al.: Global fire emissions estimates during 1997–2015, Earth Syst. Sci. Data, 9, 697–720, https://doi.org/10.5194/essd-9-697-2017, 2017.

van Marle, M. J. E., Kloster, S., Magi, B. I., Marlon, J. R., Daniau, A.-L., Field, R. D., et al.: Historic global biomass burning emissions for CMIP6 (BB4CMIP) based on merging satellite observations with proxies and fire models (1750–2015), Geosci. Model Dev., 10, 3329–3357, https://doi.org/10.5194/gmd-10-3329-2017.

Vernier, J.-P., Thomason, L. W., and Kar, J.: CALIPSO detection of an Asian tropopause aerosol layer. Geophys. Res. Lett., 38, L07804, https://doi.org/10.1029/2010GL046614, 2011.

Vernier, J.-P., Fairlie, T. D. Natarajan, M. Wienhold, F. G., Bian, J., Martinsson, B. G., Crumeyrolle, S., Thomason, L. W., and Bedka K. M.: Increase in upper tropospheric and lower stratospheric aerosol levels and its potential connection with Asian pollution, J. Geophys. Res. Atmos., 120, 1608–1619, https://doi.org/10.1002/2014JD022372, 2015.

Vernier, J.-P., Fairlie, T. D., Deshler, T., Ratnam, M. V., Gadhavi, H., Kumar, B. S., et al.: BATAL: The balloon measurement campaigns of the Asian tropopause aerosol layer. Bulletin America Meteorology Social, 99(5), 955–973. https://doi.org/10.1175/bams-d-17-0014.1, 2018.

Vogel, B., Günther, G., Müller, R., Grooß, J.-U., Hoor, P., Krämer, M., Müller, S., Zahn, A., and Riese, M.: Fast transport from Southeast Asia boundary layer sources to northern Europe: Rapid uplift in typhoons and eastward eddy shedding of the Asian monsoon anticyclone, Atmos. Chem. Phys., 14, 12,745–12,762, https://doi.org/10.5194/acp-14-12745-2014, 2014.

Wang, X., Randel, W., Pan, L., Wu, Y., Zhang, P.: Transient behavior of the Asian summer monsoon anticyclone associated with eastward eddy shedding, J. Geophys. Res.: Atmos., 127, e2021JD036090, https://doi.org/10.1029/2021JD036090, 2022.

Wright, J. S., Zhang, S., Chen, J., Davis, S. M., Konopka, P., Lu, M., Yan, X., and Zhang, G. J.: Evaluating reanalysis representations of climatological trace gas distributions in the Asian monsoon tropopause layer, Atmos. Chem. Phys., 25, 9617–9643, https://doi.org/10.5194/acp-25-9617-2025, 2025.

World Meteorological Organization (1957), Meteorology — A three-dimensional science: Second session of the Commission for Aerology, WMO Bulletin, vol. IV(no. 4), 134-138, 1957.

Yan, X., Konopka, P., Ploeger, F., Podglajen, A., Wright, J. S., Müller, R., and Riese, M.: The efficiency of transport into the stratosphere via the Asian and North American summer monsoon circulations, Atmos. Chem. Phys., 19, 15629–15649, https://doi.org/10.5194/acp-19-15629-2019, 2019.

Yu, P., Rosenlof, K. H., Liu, S., Telg, H., Thornberry, T. D., Rollins, A. W., et al.: Efficient transport of tropospheric aerosol into the stratosphere via the Asian summer monsoon anticyclone. Proceedings of the National Academy of Sciences of the United States of America, 114(27), 6972–6977, https://doi.org/10.1073/pnas.1701170114, 2017.

https://doi.org/10.5194/egusphere-2025-6257
Preprint. Discussion started: 14 January 2026

Zhang, B., Liu, H., Crawford, J. H., Chen, G., Fairlie, T. D., Chambers, S., Kang, C.-H., Williams, A. G., Zhang, K., Considine, D. B., Sulprizio, M. P., and Yantosca, R. M.: Simulation of radon-222 with the GEOS-Chem global model: emissions, seasonality, and convective transport, Atmos. Chem. Phys., 21, 1861–1887, https://doi.org/10.5194/acp-21-1861-2021, 2021.

685 Zhang, K., Feichter, H., Kazil, J., Wa, H., Zhuo, W., Griffiths, A. D., et al.: Radon activity in the lower troposphere and its impact on ionization rate: a global estimate using different radon emissions, Atmos. Chem. Phys., 11, 7817–7838, 2011. https://doi.org/10.5194/acp-11-7817-2011, 2011.

Zhang, T, Hoell, A., Perlwitz, J., Eischeid, J., Murray, D., Hoerling , M., and Hamill, T.: Towards Probabilistic Multivariate ENSO Monitoring, Geophys. Res. Lett., 46, https://doi.org/10.1029/2019GL083946, 2019.

690 Zhao, M., Golaz, J.-C., Held, I. M., Guo, H., Balaji, V., Benson, R., et al.: The GFDL global atmosphere and land model AM4.0/LM4.0: 2. Model description, sensitivity studies, and tuning strategies. Journal of Advances in Modeling Earth Systems, 10, 735-769. https://doi.org/10.1002/2017MS001209, 2018.